

Article

Decadal Prediction of the Summer Extreme Precipitation over Southern China

Huijie Wang ¹, Yanyan Huang ^{1,2,3,*}, Dapeng Zhang ¹ and Huijun Wang ^{1,2,3}

¹ Collaborative Innovation Centre on Forecast and Evaluation of Meteorological Disasters/Key Laboratory of Meteorological Disaster, Ministry of Education, Nanjing University of Information Science and Technology, Nanjing 210044, China

² Southern Marine Science and Engineering Guangdong Laboratory (Zhuhai), Zhuhai 519080, China

³ Institute of Atmospheric Physics, Nansen-Zhu International Research Centre, Chinese Academy of Sciences, Beijing 100029, China

* Correspondence: huangyy@nuist.edu.cn

Abstract: The decadal variability of the summer extreme precipitation over southern China (EPSC) is remarkable, especially for the significant decadal enhancement after the 1990s. The study documented that the summer sea surface temperature (SST) over the North Atlantic and spring sea ice concentration (SIC) over the East Siberian Sea can significantly affect the EPSC. The summer SST over the North Atlantic influences the low-pressure cyclone in the western Pacific by modulating the SST over the tropical Pacific, thus affecting EPSC. A decrease in the SIC of the East Siberian Sea induces a negative Arctic Oscillation, which induces the increased SST over northwest Pacific and the anomalous cyclone over there, in turn, affecting EPSC. Both predictors have a quasi-period of 10–14 years, which provides useful predictive signals for EPSC. The leading 7-year SST and the leading 5-year SIC are chosen to establish the prediction model based on the decadal increment method, which can well predict the EPSC, especially for the shift in the early 1990s. These results provide a clue to the limited predictability of decadal-scale extreme climate events.

Keywords: southern China; extreme precipitation; decadal prediction; decadal increment method



Citation: Wang, H.; Huang, Y.; Zhang, D.; Wang, H. Decadal Prediction of the Summer Extreme Precipitation over Southern China. *Atmosphere* **2023**, *14*, 595. <https://doi.org/10.3390/atmos14030595>

Academic Editors: Guocan Wu and Yuna Mao

Received: 22 February 2023

Revised: 16 March 2023

Accepted: 18 March 2023

Published: 21 March 2023



Copyright: © 2023 by the authors. Licensee MDPI, Basel, Switzerland. This article is an open access article distributed under the terms and conditions of the Creative Commons Attribution (CC BY) license (<https://creativecommons.org/licenses/by/4.0/>).

1. Introduction

Extreme precipitation events have attracted increasing attention due to their large impact on both the ecological environment and the social economy [1–3]. In China, extreme precipitation events occur more frequently in southern China than in other regions because the abundant rain over there [1,4]. Summer (June–August) precipitation in southern China accounts for more than 45% of the total annual precipitation. Summer also has the highest frequency of extreme precipitation events, which can lead to flooding and tremendous damage to the local economy and ecosystems [5]. For example, in mid-to-late June of 2005, persistent extreme precipitation occurred in South China with daily precipitation exceeding 400 mm, which affected 2.627 million people and caused economic losses of 3.9 billion yuan [6]. Besides the remarkable interannual variability, summer extreme precipitation over southern China has shown a significant increasing trend with a decadal enhancement in the early 1990s [7–9]. Hence, the effective and reliable prediction of the summer extreme precipitation over southern China is of great importance.

Numerous studies have revealed possible mechanisms for extreme precipitation over southern China on interannual timescales. Located in the southern coastal region of China, southern China is influenced by tropical and mid- to high-latitude climate systems such as tropical cyclones, the western North Pacific subtropical high, the East Asian subtropical westerly jet, the Asian summer monsoon, and so on [4,8,10,11]. These circulation systems can influence the extreme precipitation over southern China via the transport of water vapor and vertical motion over South China. External forcings have also been

suggested to affect the extreme precipitation over southern China. The anomalous sea surface temperature (SST) of the South China Sea and the adjacent western Pacific warm pool are linked to the extreme precipitation over southern China [12]. The variations in the SST of the Indian Ocean not only favor the maintenance of anticyclones around the Philippine Sea [13], but also affect the Pacific–Japan teleconnection pattern [14]. This, in turn, affects anomalous extreme precipitation over southern China [14,15]. The ENSO (El Niño/Southern Oscillation) and the Pacific Decadal Oscillation (PDO) are also found to be related to the decadal variations in the early summer rainfall over southern China [16]. The spring Arctic Sea ice concentration (SIC) also favors the extreme precipitation over southern China via the Eurasian teleconnection [17]. The sea ice loss along the Siberian coast influenced the precipitation anomaly in the summer of 2020 over central-east China through excessive atmospheric blockings [18].

In terms of the decadal timescale, the SST remains an important influencing factor for the decadal variability of extreme precipitation over southern China (EPSC). Zhang et al. linked the EPSC during the pre-rainy season to the decadal variation of the ENSO-like SST, which can influence the transport of water vapor via cyclonic and anticyclonic systems [19]. The anomalous SST in the western Pacific warm pool is also an important factor driving the increase in EPSC [20]. Additionally, anomalies in the latent heat flux over the South China Sea and the sensible heat flux over the Indochina peninsula are also considered important factors in EPSC [7]. However, few studies have focused on the influences of extratropical forcings on the EPSC. Moreover, the prediction of EPSC has rarely been operated. This study focuses on the mechanisms of extreme precipitation over southern China on a decadal timescale and attempts to predict its decadal variability.

Decadal prediction focuses on climate predictions over the next 1 to 10 years, which has attracted widespread attention due to its impacts on economic and social development [21]. Currently, making skillful decadal predictions based on the initialized climate models to predict precipitation over East Asia is full of challenges, especially for extreme precipitation [22–24].

Currently, decadal predictions remain challenging, and one of the important scientific issues is that the improvement of initialized climate models requires a lot of human and material resources as well as the innovation and development of related theories [23,25]. Meanwhile, some scholars have used statistical methods for decadal prediction and achieved high predictive skills. Recently, based on the interannual increment method [26], Huang and Wang proposed a new statistical approach called the decadal increment method, which can obtain decadal information by performing a 5-year running smoothing [27,28]. A statistical forecast model is then built with the 3-year decadal increment predictors, and the final prediction results can be obtained by adding the predicted increment to earlier observations. This method can increase the effective samples based on the form of decadal increment and gain useful decadal signals from the previous observations, which has shown high predictive skills in the decadal prediction of precipitation over North China, the PDO, and the East Asian summer monsoon [27–29]. Considering the frequent occurrences of extreme precipitation over southern China, this paper will first analyze the causes of the EPSC and then try to build a prediction model based on the decadal increment method. Additionally, a real-time prediction will also be given.

2. Data and Methods

2.1. Data

The daily precipitation data are from the CN05.1 gridded dataset based on 2416 station observations over China with a horizontal resolution of $(0.25^\circ \times 0.25^\circ)$ and cover the time period 1961–2021 [30]; the data are used to calculate the extreme precipitation index. The monthly mean SST data are obtained from the National Oceanic and Atmospheric Administration (NOAA) Extended Reconstructed SST V5 dataset with a horizontal resolution of $(2^\circ \times 2^\circ)$ and cover the time period 1954–2021 [31]. The monthly sea ice concentration (SIC) data are from the UK Met Office Hadley Centre with a horizontal resolution of $(1^\circ \times 1^\circ)$

and cover the time period 1954–2021 [32]. Both the SST data and SIC data are used for determining the predictors. The monthly sea-level pressure (SLP), meridional and zonal winds in 850/500/10 hPa level, and integrated water vapor flux data are obtained from the ERA5 reanalysis dataset of the European Centre for Medium-Range Weather Forecasts with a horizontal resolution of ($1^\circ \times 1^\circ$) and cover the time period 1950–2021 [33]; they are used to analyze the mechanisms of SST and SIC affecting the EPSC. The monthly AMO data during 1946–2021 and PDO data during 1946–2019 are obtained from the NCAR Climate Data and are used to analyze their potential correlation with the EPSC.

2.2. Definition of the Extreme Precipitation Index

According to the recommendation of the Expert Team on Climate Change Detection and Indices (ETCCDI, <http://cccma.seos.uvic.ca/ETCCDI/indices.shtml>, accessed on 15 March 2021), the summer extreme precipitation index (R95p) is defined as the total amount of precipitation on days with daily precipitation (daily precipitation ≥ 0.1 mm) larger than the 95th percentile of the summer (June–August) daily precipitation.

2.3. Methods

The decadal variability of extreme precipitation is obtained by performing a 5-year running mean of regional averaged extreme precipitation. The 5-year running mean of regional averaged extreme precipitation over southern China is defined as the decadal variability of the southern China extreme precipitation (EPSC) index. The 3-year decadal increment of the EPSC (DI_EPSC) is the predictand, which is defined as the EPSC of the current year minus the EPSC at 3 years ago (Equation (1)). The final predicted EPSC can be obtained by adding the predicted DI_EPSC to the observed EPSC from 3 years ago (Equation (2)). The main predictors are determined by the stepwise regression with the F-test at the 95% confidence level, which must be well-correlated with the predictand and independent of each other. The multiple linear regression method is applied to build the statistical model with the determined predictors in the form of a 3-year decadal increment. To prevent the prediction model from using information from any prediction period, predictors are at least 3 years ahead of the predictand.

$$DI_EPSC_i = EPSC_i - EPSC_{i-3} \quad (1)$$

$$EPSC_i = EPSC_{i-3}^{obs} + DI_EPSC_i^{s-model} \quad (2)$$

To verify the prediction skills of the statistical model, cross-validation and independent hindcast are applied. In the cross-validation, the observational data of the EPSC during 1966–2018 are selected to predict the DI_EPSC for the target year. Noteworthy, the statistical model is built by leaving 5 years out (from 2 years before to 2 years after the target year for the DI_EPSC and the leading 5 years for the predictors). The same observational data are also used in the independent hindcast. The statistical model is established to predict the DI_EPSC for the target year with the data from 43 years to 3 years leading the target year. This process is repeated from 2009 to 2018. For instance, the predictand during 1966–2006 and the predictors during 1963–2003 are chosen to build the statistical model to predict the DI_EPSC for 2009.

Empirical orthogonal function (EOF) analysis is a linear data transformation defined in terms of the eigenvectors of their covariance matrix [34]. In this study, it is applied to investigate the decadal variation of extreme precipitation over southern China.

The significance of the correlation coefficient is examined by the Student's *t*-test. The effective sample size N^* is calculated as follows [35]:

$$N^* = N \frac{1 - r_1 r_2}{1 + r_1 r_2} \quad (3)$$

where N is the number of available time steps, and r_1 and r_2 are the autocorrelation coefficients of the two variables lagged by one step.

The mean square skill score ($MSSS$) is used to measure the predictive skill of the statistical model [36] and is calculated as follows:

$$MSSS = 1 - \frac{MSE}{MSE_c} \quad (4)$$

$$MSE = \frac{1}{n} \sum_{i=1}^n (f_i - o_i)^2 \quad (5)$$

$$MSE_c = \frac{1}{n} \sum_{i=1}^n (o_i - \bar{o})^2 \quad (6)$$

where f_i and o_i represent the time series of the observations and forecasts, respectively. $MSSS$ is the percentage reduction of the mean square error (MSE) predicted by the statistical model, and MSE_c is the MSE of the climatological forecast. A positive skill means that the statistical model forecast is better than the climatology forecast.

3. Results

3.1. Decadal Variation

Figure 1 shows the spatial pattern of the first EOF mode of the decadal variation of summer extreme precipitation in East China during 1963–2018. The spatial pattern of the first EOF mode can explain 21.6% of the total variance of summer extreme precipitation in East China. There is abundant extreme precipitation occurred over southern China compared to other regions (Figure 1a), which has been noticed by previous studies [1]. Since there is a uniform spatial pattern over southern China (22° – 30° N, 107° – 120° E), the 5-year running mean of regional averaged summer extreme precipitation over southern China is defined as the decadal variability of the extreme precipitation over southern China (EPSC) index (Figure 1b). The EPSC has an increasing trend with a significant shift after the 1990s [7–9]. The time series of the leading EOF mode (PC1) correlates well with the EPSC with a correlation coefficient of 0.94, indicating that the EPSC index can reasonably reflect the decadal variability of extreme precipitation over southern China. Moreover, the 3-year decadal increment of the EPSC (DI_EPSC) is then calculated, which will be treated as the predictand in the following section.

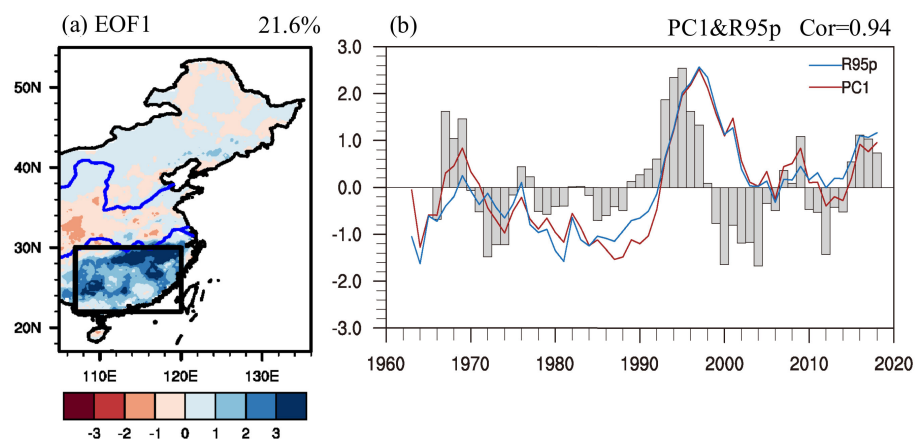


Figure 1. (a) The spatial pattern of the leading EOF mode and (b) the corresponding normalized time series of the 5-year smoothing mean of the total summer extreme precipitation in East China during 1963–2018 (PC1, red line), as well as the time series of the EPSC (R95p, blue line) and DI_EPSC during 1966–2018. EPSC is defined as the 5-year running mean of regional averaged summer extreme precipitation over southern China. DI_EPSC is calculated as the 3-year decadal increment of the EPSC.

3.2. Predictors

This section mainly discusses the predictors of EPSC and the associated mechanisms. Based on previous studies, potential predictors are chosen mainly from external forcings, including the SST, the SIC, the soil moisture, and the snow depth. The stepwise regression with the F-test at the 95% confidence level is used to determine the main predictors of EPSC. The determined decadal predictors must be well-correlated with the predictand and independent of each other. Two final predictors, including the summer SST of the North Atlantic leading the DI_EPSC by 7 years and the spring SIC near the East Siberian Sea leading the DI_EPSC by 5 years, which are well-correlated with the DI_EPSC and independent of each other, are therefore chosen to predict the decadal summer EPSC. The physical processes of these two predictors affecting the EPSC will be explored in detail.

Previous studies have shown that triple or dipolar SST anomalies in the North Atlantic can induce a wave train over the North Atlantic through Eurasia, which is one of the factors influencing precipitation and extreme precipitation in eastern China [37–40]. Additionally, anomalous warming in the North Atlantic can also induce cooling in the tropical eastern Pacific Ocean and warming in the Indo-Pacific Ocean through a series of air–sea interactions [22,40–44]. This is a significant factor in maintaining an anticyclone over the western Pacific and transporting water vapor to eastern China [40], thus affecting extreme precipitation over southern China.

Notably, the leading 7-year summer (June–August) SST over the North Atlantic is significantly related to the EPSC (Figure 2a). There significant positive and negative centers emerged in the mid- to high-latitude regions of the North Atlantic, indicating the influence of the SST dipole over the North Atlantic ahead 7 years on the EPSC. The SST index (DI_SST) is therefore defined as the regional averaged decadal increment in the SST over the positive region (26°–39° N, 43°–60° W) minus that of the negative region (49°–57° N, 14°–49° W).

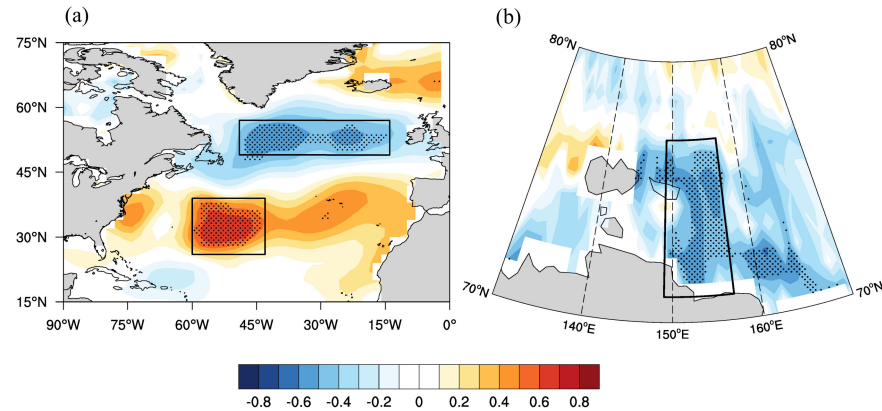


Figure 2. Spatial pattern of correlation coefficients between the predictand (DI_EPSC) during the time period 1966–2018 and the predictors: (a) the 3-year increment of the summer SST 7 years ahead of the DI_EPSC during 1959–2011, (b) the 3-year increment of the spring SIC 5 years ahead of DI_EPSC during 1961–2013. The dotted regions indicate significant variability at the 95% confidence level based on the Student’s *t*-test. The rectangles indicate the area-weighted averaged regions of the predictors, including the DI_SST (26°–39° N, 43°–60° W minus 49°–57° N, 14°–49° W), and the DI_SIC (71°–77° N, 149°–157° E).

How do the SST anomalies affect EPSC 7 years in advance? The wavelet analysis of the DI_SST during 1959–2011 is shown in Figure 3a, which indicates that the dipole anomalies of the North Atlantic SST have a quasi-period of 12–14 years (Figure 3a) with a significant negative autocorrelation of 5–7 years (Figure 3b). Both the period and significant auto-correlation imply that the dipole SST anomalies of the North Atlantic can provide useful predictive information for EPSC 7 years ahead.

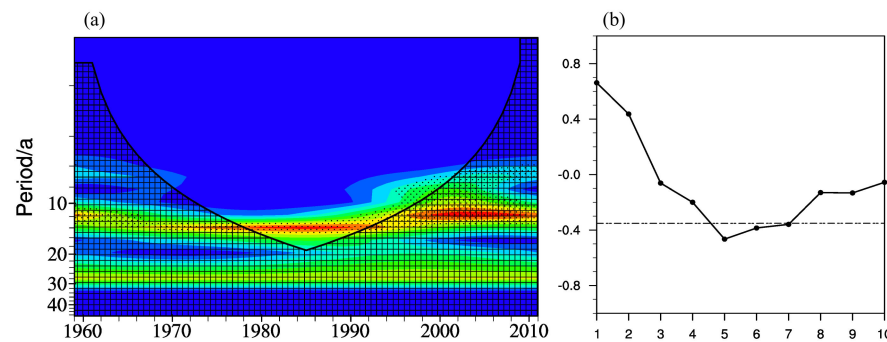


Figure 3. (a) Wavelet analysis and (b) the autocorrelation coefficients of the DI_SST predictor. In Panel (a), the dotted regions indicate significant variability at the 95% confidence level. In Panel (b), the horizontal coordinates indicate the years lagged by the predictors and the dashed lines indicate significant variability at the 90% confidence level. Additionally, the effective sample size is 21.

What are the specific physical processes by which the SST dipole pattern over the North Atlantic affects EPSC?

Figure 4a shows the spatial pattern of the correlation coefficient between the DI_SST and surface winds. The SST dipole over the North Atlantic can lead to significant anomalous easterlies from the tropical North Atlantic to the tropical East Pacific (as shown in the rectangle region of Figure 4a). The northeasterly/easterly anomalies (as shown in the rectangle region of Figure 4b) favor cooling in the tropical eastern Pacific and warming in the western Pacific SST (Figure 4b). This SST pattern can enhance the Walker circulation, which is characterized by descending motion over the eastern Pacific and ascending motion over the western Pacific (Figure 4c). There are associated cyclonic anomalies over the northwestern Pacific in both low troposphere to mid troposphere (Figure 4d,e). In the west of the cyclone, significant northeasterly winds prevail over southern China. In the mid troposphere, there are significant easterly winds from southern China to Tibetan Plateau (Figure 4e), which may generate descent motion (Figure 4f) through the zonal temperature gradient between southern China and Tibetan Plateau [45–47]. Both the northeasterly winds and descending motion is unfavorable for the increase of EPSC [48,49]. Thus, the preceding 7-year SST dipole pattern over the North Atlantic is chosen to be one predictor for EPSC based on its significant influence and period of 12–14 years.

In addition, previous studies have also explored the connection between the decrease in spring Arctic SIC and the increase in summer precipitation even extreme precipitation in East and southern China [17,18,50]. The decrease in Arctic SIC can induce a Eurasia teleconnection, which is inductive to transport water vapor to southern China [17]. In this paper, the leading 5-year spring SIC near the East Siberian Sea also influences the EPSC. Figure 2b shows a significant negative center near the East Siberian Sea, which indicates the influence of the SIC over the East Siberian Sea ahead of 5 years on EPSC. Hence, the SIC index (DI_SIC) is defined as the regional averaged decadal increment in the SIC over the negative region (71° – 77° N, 149° – 157° E).

How do the SIC anomalies influence EPSC 5 years in advance? As shown in Figure 5, the DI_SIC has a quasi-period of 10 years with a significant negative autocorrelation of 5–6 years (Figure 5b). Both the period and the significant autocorrelation indicate that the SIC anomalies of the East Siberian Sea can also provide useful predictive information for EPSC 5 years in advance.

How can the SIC over the East Siberian Sea physically influence EPSC?

Figure 6a shows the spatial pattern of the correlation coefficient between the DI_SIC and the spring SLP, which is similar to the Arctic Oscillation (AO) pattern. When the SIC in the East Siberian decreases, the local surface temperature increases, which makes the temperature differences between the pole and mid latitudes' decrease, and AO accordingly shows a negative phase. This is consistent with previous studies [51,52]. When SIC in the East Siberian decreases, there appears to be a significant warming of the anomalous SST

near the North Pacific under the influence of AO (Figure 6b). The anomalous increased SST can store useful information from spring to summer, which, in turn, induces cyclonic anomalies over the northwest Pacific (Figure 6c). The northerly in the west of the cyclone can weaken the water vapor transport to southern China, where the water vapor flux appears to be significantly divergent (Figure 6e). Figure 6d shows the negative correlation of DI_SIC with the vertical motion of southern China. When the sea ice decreases, there is descending motion in southern China, which may be generated from the divergent motion. Both the descending motion and divergent water vapor flux are unfavorable for the increase of EPSC. These findings are consistent with previous studies, which found that an anomalous AO can enhance the connection between the warm SST in the North Pacific and the cyclone in the northwest Pacific, thus affecting the summer climate in East Asia [53,54]. Thus, the preceding 5-year SIC in the East Siberian Sea is chosen to be the other predictor for EPSC based on its significant effects on EPSC and its period of 10 years.

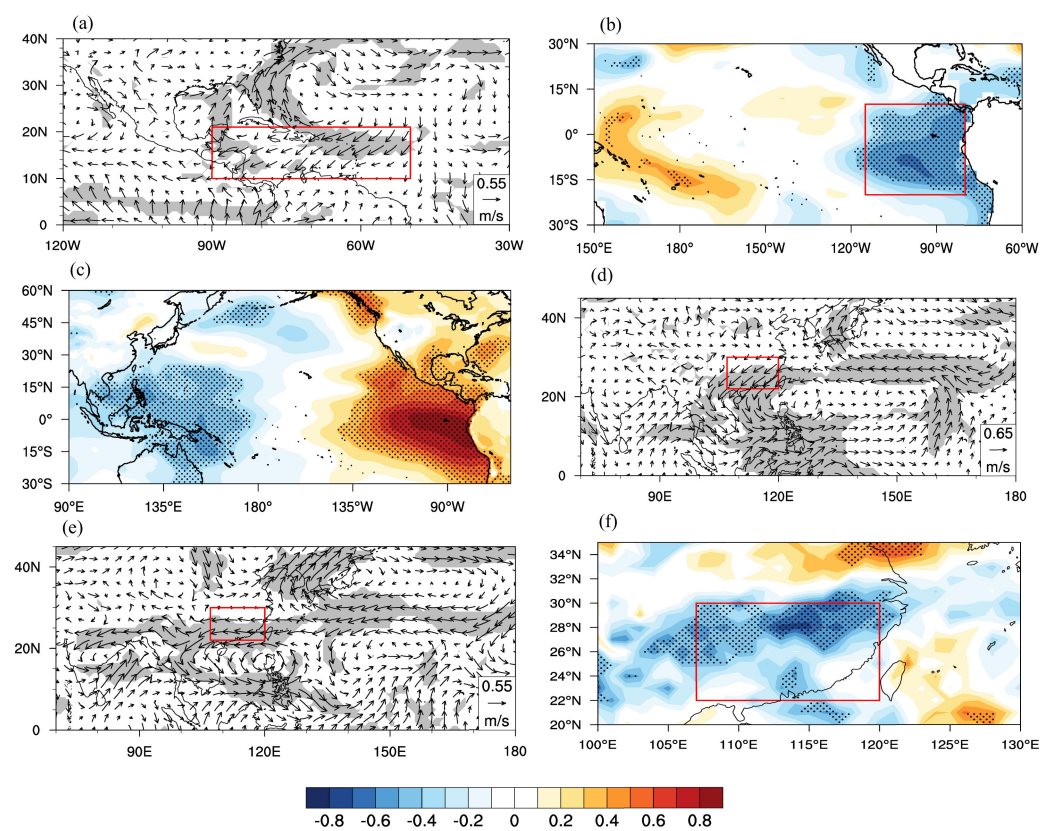


Figure 4. Correlation coefficients between the DI_SST with (a) the summer surface winds, (b) the SST, (d) the 850 hPa winds, and (e) the 500 hPa winds during 1959–2011. Correlation coefficients between the eastern Pacific SST (red rectangle region in Panel (b), SST is multiplied by -1) with (c) the mean SLP during 1959–2011. Correlation coefficients between the DI_SST during 1959–2011 with (f) the 500 hPa vertical velocity during 1966–2018. Thus, the negative value in (f) should indicate the descent motion due to the negative autocorrelation with a lag of 7 years. The dotted regions and shaded regions indicate significant variability at the 90% confidence level, and the red rectangle region in Panels (d–f) is the study area (southern China). The variables including SST, surface winds, SLP, 850 hPa winds, 500 hPa winds, and 500 hPa vertical velocity are in the form of a 3-year decadal increment.

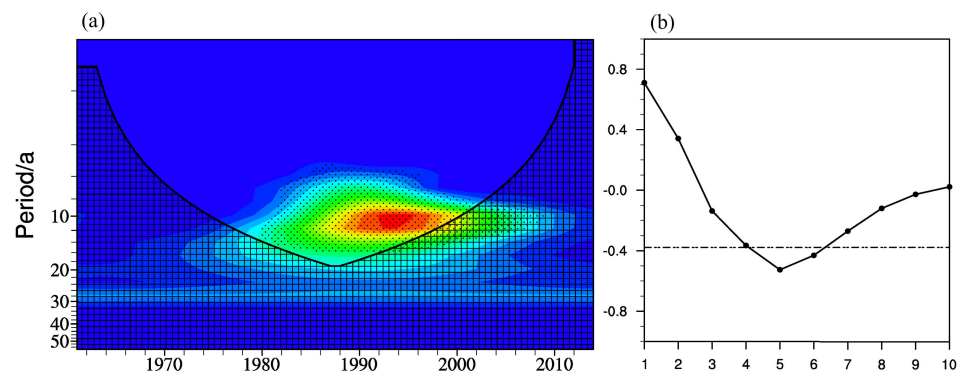


Figure 5. (a) Wavelet analysis and (b) the autocorrelation coefficients of the DI_SIC predictor. In Panel (a), the dotted regions indicate significant variability at the 95% confidence level. In Panel (b), the horizontal coordinates indicate the years lagged by the predictors and the dashed lines indicate significant variability at the 90% confidence level. Additionally, the effective sample size is 18.

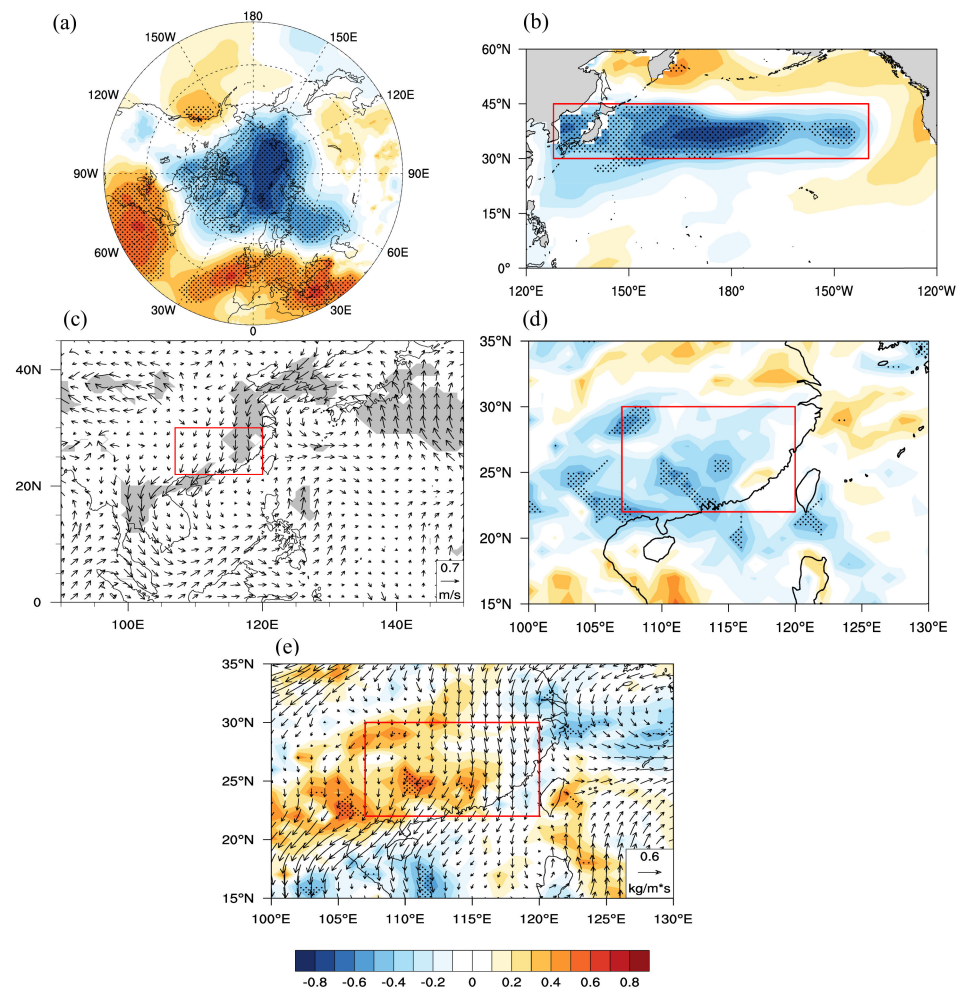


Figure 6. Correlation coefficients between the DI_SIC with (a) the spring SLP, (b) the SST, and (d) 500 hPa vertical velocity during 1961–2013. Correlation coefficients between the SST over North Pacific (red rectangle region of Panel (b)), with the summer (c) 850 hPa winds and (e) vertical integral of the divergence of the water vapor flux during 1961–2013. The dotted and shaded regions indicate significant variability at the 90% confidence level, and the red rectangle region of Panels (c,d) represent the study area (southern China). The variables including SST, SLP, 850 hPa winds, 500 hPa vertical velocity, and vertical integral of the divergence of the water vapor flux are in the form of a 3-year decadal increment.

3.3. Decadal Prediction Model

The two predictors mentioned above, including the DI_{SST} and DI_{SIC} , have significant influences on the predictand (DI_{EPSC}) with correlation coefficients of 0.79 and -0.51 , respectively (Figure 7). The two predictors are generally independent of each other with the correlation coefficient of -0.2 , which is not statistically significant. The multiple linear regression method is therefore applied to build the statistical model for predicting the DI_{EPSC} based on the DI_{SST} and DI_{SIC} .

$$DI_{EPSC} = 0.71 \times DI_{SST} - 0.36 \times DI_{SIC} \quad (7)$$

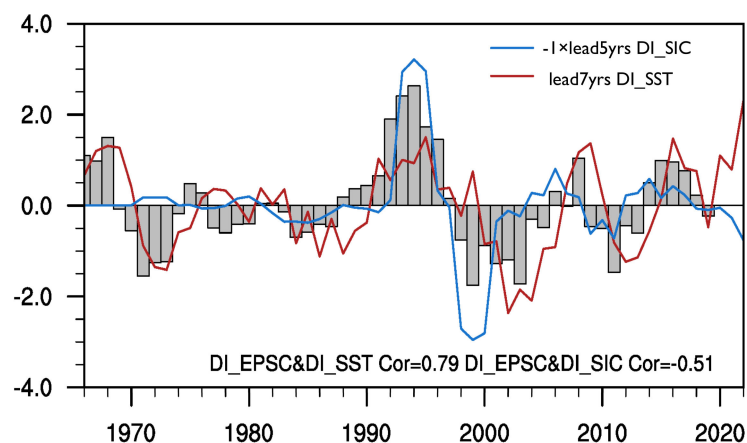


Figure 7. Time series of the DI_{EPSC} during 1966–2019 (bars), the leading 7-year DI_{SST} during 1959–2015 (red line), and the leading 5-year DI_{SIC} during 1961–2017 (blue line). The results in this figure were standardized.

The main factor affecting summer EPSC is the summer SST in the North Atlantic, which explains 50% of the variance of the DI_{EPSC} . The second factor is the spring SIC in the East Siberian Sea, which explains 13% of the variance of the DI_{EPSC} .

Cross-validation and independent hindcast are applied to measure the prediction skill of the statistical model. The results of cross-validation (Figure 8a) show that the predicted DI_{EPSC} is significantly related to the observed DI_{EPSC} , with a correlation coefficient of 0.83 and an MSSS of 0.69. The phase of the predicted DI_{EPSC} is consistent with that of the observed DI_{EPSC} in most years, apart from the time period 1976–1982. The predicted DI_{EPSC} effectively captures the variability of the observed DI_{EPSC} , especially in recent years. The final predicted EPSC is obtained by adding the predicted DI_{EPSC} to the observed EPSC 3 years ago (Figure 8c). The final predicted EPSC also shows a high consistency with the observed EPSC, with a correlation coefficient of 0.86 and an MSSS of 0.72. The phase of the predicted EPSC is consistent with that of the observed EPSC in most years, although the extreme values in the 1990s are not captured well by this model. Noteworthy, the final predicted EPSC captures the shift in the early 1990s. The other decadal shifts with small fluctuations are also well-captured by this statistical model.

From the independent hindcast results (Figure 8b), the predicted DI_{EPSC} is also consistent with the observed DI_{EPSC} , with a significant correlation coefficient of 0.9 and an MSSS of 0.81. The phase between the predicted DI_{EPSC} and the observed DI_{EPSC} is generally consistent in most years except 2010. The predicted DI_{EPSC} can also effectively capture the variability and amplitude of the observed DI_{EPSC} . Additionally, the extreme value of the DI_{EPSC} in 2016 is captured by this model. The shift during 2014–2015 is also captured by this model. The final predicted EPSC also shows high consistency with the observed EPSC, with a correlation coefficient of 0.78 and an MSSS of 0.52 (Figure 8d). The phase of the predicted EPSC is generally consistent with the phase of the observed EPSC in most years apart from 2012 and 2015. The variability and amplitude between the predicted

EPSC and the observed EPSC are also generally consistent in most years, although there are small deviations, which shows generally high prediction skills.

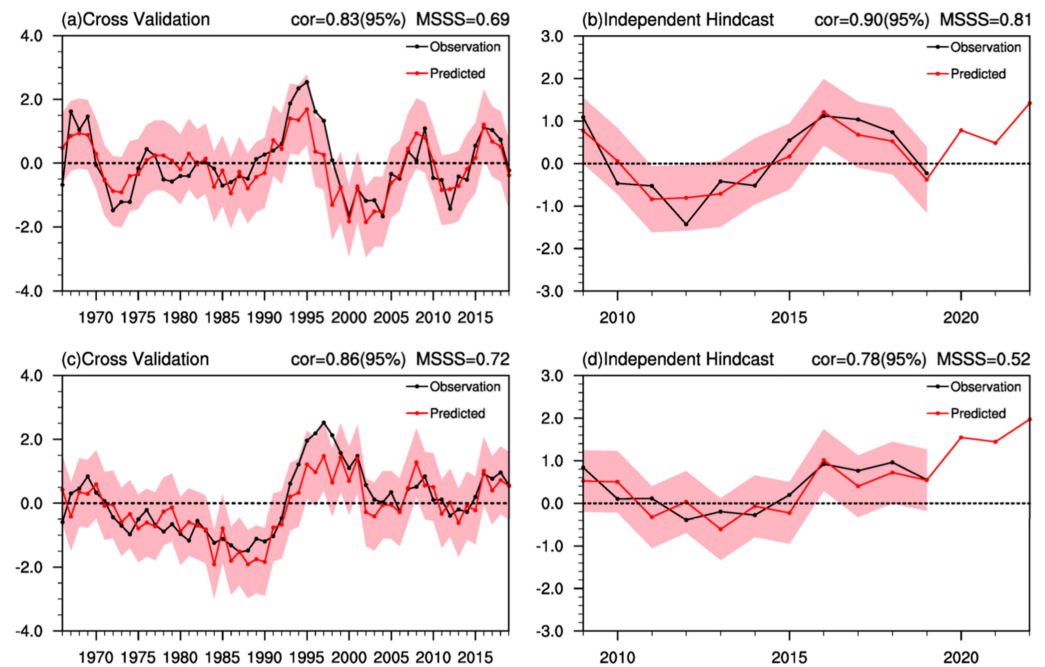


Figure 8. The results of the cross-validation for the period of 1966–2019 (a,c) and the independent hindcast for the period of 2009–2019 (b,d). The panels show the decadal increment of the EPSC (DI_EPSC) predicted by the statistical model (a,b); the final predicted EPSC, achieved by adding the predicted DI_EPSC to the observed EPSC at 3 years ago (c,d), where the light pink regions indicate significant variability at the 95% prediction interval. The results in this figure were standardized. Cor indicates the correlation coefficient between the observations and the prediction results, and the MSSS is the prediction skill of the statistical model.

3.4. Real-Time Prediction

The results of the cross-validation and independent hindcast show that this statistical model has reasonable skills in predicting the EPSC, including the shift, phase, and amplitude. Thus, in this section, we further try to make a real-time prediction of EPSC.

Figure 7 indicates that there are remarkable positive anomalies in DI_SST and slight negative anomalies in DI_SIC during 2020–2022. Since the percentage of the explained variance from DI_SST (50%) is higher than that from the DI_SIC (13%) and the anomalous amplitude is also higher in DI_SST than that in DI_SIC, DI_EPSC would increase during 2020–2022 (Figure 8b). As shown in Figure 8d, the real-time predicted EPSC is in a positive phase during 2020–2022, indicating that EPSC would increase during 2020–2022, with a remarkable increase in 2022. Figure 9 shows the observed recent 5-years running mean of the summer extreme precipitation over Eastern China, there are remarkable positive anomalies over Southern China. Noteworthy, the historic Dragon-Boat extreme precipitation event occurred in southern China in May–June 2022 [55], which is consistent with the real-time prediction results. Thus, this statistical model can therefore predict the real-time results 3 years in advance and shows confidence in the future prediction of EPSC.

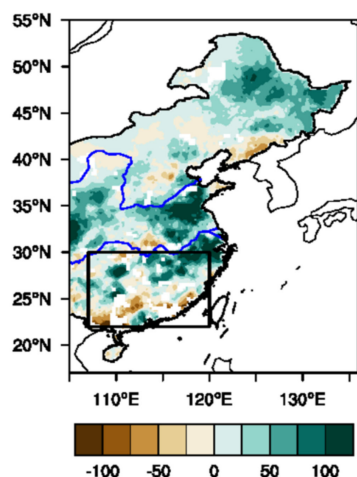


Figure 9. Spatial pattern of the anomaly extreme precipitation (unit: mm) over eastern China after a 5-year running mean in 2019 related to the climatology (1991–2020). The black rectangle region represents the study area (southern China).

4. Discussion

Previous studies show that PDO and AMO have significant effects on the decadal summer rainfall over East China [56], which may provide useful information for the prediction of EPSC. We also attempted to use PDO and AMO as predictors. However, the correlations between the PDO/AMO with EPSC are not statistically significant at the 95% confidence level, especially in the decadal increment form, no matter the simultaneous or leading correlations. The results are also true in DI form (Table 1). The above results will not change when using other seasonal mean PDO/AMO predictors. One possible reason is that the extreme precipitation is discussed in this study compared to the normal precipitation in previous research. The other reason is that the DI_SST/DI_SIC suggested in this study may play the role of bridge for the influence of PDO/AMO on EPSC. Therefore, these two predictors contribute more significantly to the EPSC and predict the EPSC better than PDO and AMO.

Table 1. The correlation coefficients between the EPSC and the leading 3–7 years summer PDO/AMO. The value in parentheses indicates the correlation coefficient in decadal increment (DI) form.

	Leading 3 Years	Leading 4 Years	Leading 5 Years	Leading 6 Years	Leading 7 Years
PDO	0.23 (0.39)	0.21 (0.24)	0.16 (−0.06)	0.15 (−0.26)	0.19 (−0.39)
AMO	0.30 (−0.33)	0.30 (−0.29)	0.31 (−0.22)	0.33 (−0.09)	0.36 (−0.05)

5. Conclusions

This paper analyzed the summer EPSC and explored the main influencing factors. The summer extreme precipitation over southern China has been increasing over recent decades, with a significant shift in the early 1990s. The summer SST of the North Atlantic and the spring SIC in the East Siberian Sea are indicated to affect the EPSC. Both predictors have a quasi-period of 10–14 years, which can provide useful prediction information for summer EPSC leading 5–7 years. Therefore, these two predictors were chosen to establish the prediction model based on the decadal increment method.

Both the cross-validation and independent hindcast results illustrate that the decadal increment method can predict the EPSC well, especially the shift in the early 1990s. Additionally, the real-time prediction results show that the EPSC would increase during 2020–2022, which is consistent with the actual situation of more EPSC. These prediction results will help with future local disaster prevention and mitigation.

The decadal increment method not only adds leading observational data to obtain useful decadal information, but also adds valid samples in the correlation analysis, which predicts the summer EPSC well. This statistical approach provides new ideas for the current decadal climate prediction, especially decadal changes. In the future, the statistical-dynamical model or machine learning combined with the increment method can also be attempted to improve decadal predictions.

Author Contributions: Conceptualization, H.W. (Huijun Wang), Y.H. and H.W. (Huijie Wang); Software, H.W. (Huijie Wang); Writing—original draft, H.W. (Huijie Wang); Writing—review and editing, Y.H. and D.Z. All authors have read and agreed to the published version of the manuscript.

Funding: This work was supported by the National Natural Science Foundation of China (Grant Nos. 42088101 and 41991283).

Institutional Review Board Statement: Not applicable.

Informed Consent Statement: Not applicable.

Data Availability Statement: The NOAA SST data are obtained from <http://www.esrl.noaa.gov/psd/data/gridded/data.noaa.ersst.v5.html> (accessed on 15 March 2021). The Hadley sea ice concentration data are from <https://www.metoffice.gov.uk/hadobs/hadisst/data/download.html> (accessed on 15 March 2021). The ERA5 reanalysis dataset of the European Centre for Medium-Range Weather Forecasts are available at <https://cds.climate.copernicus.eu/cdsapp#!/search?type=dataset&text=ERA5> (accessed on 15 March 2021). The NCAR Climate (PDO, AMO) data and instructions are obtained from <https://climatedataguide.ucar.edu/climate-data> (accessed on 10 October 2022).

Acknowledgments: The authors are very grateful to the editor and anonymous reviewers for their help and recommendations. Thanks for the support of the National Natural Science Foundation of China (Grant No. 41991283).

Conflicts of Interest: The authors declare no conflict of interest.

References

1. Zhai, P.; Zhang, X.; Wan, H.; Pan, X. Trends in Total Precipitation and Frequency of Daily Precipitation Extremes over China. *J. Clim.* **2005**, *18*, 1096–1108. [\[CrossRef\]](#)
2. Sun, J. The contribution of extreme precipitation to the total precipitation in China. *Atmos. Ocean. Sci. Lett.* **2012**, *5*, 499–503.
3. Zheng, G.; Yang, L.; Chen, Q.; Zhou, X. The increasing predominance of extreme precipitation in Southwest China since the late 1970s. *Atmos. Ocean. Sci. Lett.* **2022**, *15*, 100227. [\[CrossRef\]](#)
4. Cui, D.; Wang, C.; Santisirisomboon, J. Characteristics of extreme precipitation over eastern Asia and its possible connections with Asian summer monsoon activity. *Int. J. Climatol.* **2019**, *39*, 711–723. [\[CrossRef\]](#)
5. Zhang, T.; Wei, F. Probability distribution of precipitation extremes during raining seasons in South China. *Acta Meteorol. Sin.* **2009**, *67*, 442–451.
6. Lin, A.; Liang, J.; Li, C.; Gu, D. Monsoon circulation background of ‘0506’ continuous rainstorm in South China. *Adv. Water Sci.* **2007**, *18*, 424–434.
7. Ning, L.; Qian, Y. Interdecadal change in extreme precipitation over South China and its mechanism. *Adv. Atmos. Sci.* **2009**, *26*, 109–118. [\[CrossRef\]](#)
8. Li, H.; Chen, H.; Wang, H. Changes in clustered extreme precipitation events in South China and associated atmospheric circulations. *Int. J. Climatol.* **2016**, *36*, 3226–3236. [\[CrossRef\]](#)
9. He, L.; Hao, X.; Han, T. How do extreme summer precipitation events over eastern China subregions change? *Geophys. Res. Lett.* **2021**, *48*, e2020GL091849. [\[CrossRef\]](#)
10. Xiang, B.; Dong, X.; Li, Y. Climate change trend and causes of tropical cyclones affecting the South China Sea during the past 50 years. *Atmos. Ocean. Sci. Lett.* **2020**, *13*, 301–307. [\[CrossRef\]](#)
11. Zhou, Y.; Yuan, J.; Wen, Z.; Huang, S.; Chen, X.; Guo, Y.; Lin, Q. The impacts of the East Asian subtropical westerly jet on weather extremes over China in early and late summer. *Atmos. Ocean. Sci. Lett.* **2022**, *15*, 100212. [\[CrossRef\]](#)
12. Qi, Q.; Cai, R.; Zhang, Q. Primarily analyses on variations of summer extreme precipitation in South China and its relation to the sea-air anomaly in Northwestern Pacific Ocean. *Plateau Meteorol.* **2013**, *32*, 110–121.
13. Xie, S.-P.; Hu, K.; Hafner, J.; Tokinaga, H.; Du, Y.; Huang, G.; Sampe, T. Indian Ocean capacitor effect on Indo-western Pacific climate during the summer following El Niño. *J. Clim.* **2009**, *22*, 730–747. [\[CrossRef\]](#)
14. Zhong, Y.; Yang, M.; Yuan, C. Temporal and spatial characteristics of summer extreme precipitation in Eastern China and possible causalities. *J. Geosci. Environ. Prot.* **2020**, *8*, 36–46. [\[CrossRef\]](#)
15. Li, J.; Wang, B. Predictability of summer extreme precipitation days over eastern China. *Clim. Dyn.* **2018**, *51*, 4543–4554. [\[CrossRef\]](#)

16. Chan, J.; Zhou, W. PDO, ENSO and the early summer monsoon rainfall over south China. *Geophys. Res. Lett.* **2005**, *32*. [[CrossRef](#)]
17. Xu, H.; Chen, H.; Wang, H. Interannual variation in summer extreme precipitation over Southwestern China and the possible associated mechanisms. *Int. J. Climatol.* **2021**, *41*, 3425–3438. [[CrossRef](#)]
18. Chen, X.; Dai, A.; Wen, Z.; Song, Y. Contributions of Arctic sea-ice loss and East Siberian atmospheric blocking to 2020 rec-ord-breaking Meiyu-Baiu rainfall. *Geophys. Res. Lett.* **2021**, *48*, e2021GL092748.
19. Zhang, K.; Li, L.; Cheng, S. Analysis of interdecadal variation of precipitation and impact factors during the pre-rainy season in South China. *J. Arid. Meteorol.* **2016**, *34*, 64–74.
20. Yang, H.; Gong, Z.; Wang, X.; Feng, G. Analysis of the characteristics and causes of interdecadal changes in the summer extreme precipitation over Eastern China. *Chin. J. Atmos. Sci.* **2021**, *45*, 683–696.
21. Meehl, G.A.; Goddard, L.; Murphy, J.; Stouffer, R.; Boer, G. Decadal prediction: Can it be skillful? *Bull. Amer. Meteorol. Soc.* **2009**, *90*, 1467–1486. [[CrossRef](#)]
22. Monerie, P.A.; Robson, J.; Dong, B.; Dunstone, N. A role of the Atlantic Ocean in predicting summer surface air temperature over North East Asia? *Clim. Dyn.* **2018**, *51*, 473–491. [[CrossRef](#)]
23. Smith, D.M.; Eade, R.; Scaife, A.A.; Caron, L. Robust skill of decadal climate predictions. *Npj Clim. Atmos. Sci.* **2019**, *2*, 13. [[CrossRef](#)]
24. Dunstone, N.; Smith, D.; Yeager, S. Skilful interannual climate prediction from two large initialised model ensembles. *Environ. Res. Lett.* **2020**, *15*, 094083. [[CrossRef](#)]
25. Doblas-Reyes, F.J.; Andreu-Burillo, L.; Chikamoto, Y.; García-Serrano, J. Initialized near-term regional climate change prediction. *Nat. Commun.* **2013**, *4*, 1715. [[CrossRef](#)]
26. Huang, Y.; Wang, H.; Fan, K. Improving the prediction of the summer Asian-Pacific Oscillation using the interannual increment approach. *J. Clim.* **2014**, *27*, 8126–8134. [[CrossRef](#)]
27. Huang, Y.; Wang, H. Is the Regional Precipitation Predictable in Decadal Scale? A Possible Approach for the Decadal Prediction of the Summer Precipitation Over North China. *Earth Space Sci.* **2020**, *7*, e2019EA000986. [[CrossRef](#)]
28. Huang, Y.; Wang, H. A possible approach for the decadal prediction of PDO. *Acta Meteorol. Sin.* **2020**, *78*, 177–186. [[CrossRef](#)]
29. Qian, D.; Huang, Y.; Wang, H. A preliminary attempt on decadal prediction of the East Asian summer monsoon. *Theor. Appl. Climatol.* **2022**, *148*, 1499–1511. [[CrossRef](#)]
30. Wu, J.; Gao, X. A gridded daily observation dataset over China region and comparison with the other datasets. *Chin. J. Geophys.* **2013**, *56*, 1102–1111.
31. Huang, B.; Thorne, P.W.; Banzon, V.F.; Boyer, T. Extended Reconstructed Sea Surface Temperature, Version 5 (ERSSTv5): Upgrades, Validations, and Intercomparisons. *J. Clim.* **2017**, *30*, 8179–8205. [[CrossRef](#)]
32. Rayner, N.A.; Parker, D.; Horton, E.B.; Folland, C. Global analyses of sea surface temperature, sea ice, and night marine air temperature since the late nineteenth century. *J. Geophys. Res.* **2003**, *108*, 4407. [[CrossRef](#)]
33. Hersbach, H.; Bell, B.; Berrisford, P.; Hirahara, S. The ERA5 global reanalysis. *Quart. J. Roy. Meteorol. Soc.* **2020**, *146*, 1999–2049. [[CrossRef](#)]
34. Wilks, D.S. Principal component (EOF) analysis. *Int. Geophys.* **2011**, *100*, 519–562.
35. Bretherton, C.S.; Widmann, M.; Dymnikov, V.P.; Wallace, J. The effective number of spatial degrees of freedom of a time-varying field. *J. Clim.* **1999**, *12*, 1990–2009. [[CrossRef](#)]
36. Murphy, A.H. Skill scores based on the mean square error and their relationships to the correlation coefficient. *Mon. Weather Rev.* **1988**, *116*, 2417–2424. [[CrossRef](#)]
37. Chen, J.; Wen, Z.; Wu, R.; Wang, X.; He, C.; Chen, Z. An interdecadal change in the intensity of interannual variability in summer rainfall over southern China around early 1990s. *Clim. Dyn.* **2017**, *48*, 191–207. [[CrossRef](#)]
38. Lü, J.; Li, Y.; Zhai, P.; Chen, J. Teleconnection patterns impacting on the summer consecutive extreme rainfall in Central-Eastern China. *Int. J. Climatol.* **2017**, *37*, 3367–3380. [[CrossRef](#)]
39. Sun, X.; Li, S.; Hong, X.; Lu, R. Simulated Influence of the Atlantic Multidecadal Oscillation on Summer Eurasian Nonuniform Warming since the Mid-1990s. *Adv. Atmos. Sci.* **2019**, *36*, 811–822. [[CrossRef](#)]
40. Chen, L.; Li, G.; Lu, B.; Li, Y.; Gao, C.; Long, S.-M.; Li, X.; Wang, Z. Two approaches of the spring North Atlantic sea surface temperature affecting the following July precipitation over central China: The tropical and extratropical pathways. *J. Clim.* **2022**, *35*, 2969–2986. [[CrossRef](#)]
41. McGregor, S.; Timmermann, A.; Stuecker, M.F.; England, M. Recent Walker circulation strengthening and Pacific cooling amplified by Atlantic warming. *Nat. Clim. Chang.* **2014**, *4*, 888–892. [[CrossRef](#)]
42. Cai, W.; Wu, L.; Lengaigne, M.; Li, T.; McGregor, S.; Kug, J.-S.; Yu, J.-Y.; Stuecker, M.F.; Santoso, A.; Li, X.; et al. Pantropical climate interactions. *Science* **2019**, *363*, eaav4236. [[CrossRef](#)] [[PubMed](#)]
43. Ham, Y.; Kug, J.; Park, J.; Jin, F. Sea surface temperature in the north tropical Atlantic as a trigger for El Niño/Southern Oscillation events. *Nat. Geosci.* **2013**, *6*, 112–116. [[CrossRef](#)]
44. Zhang, W.; Jiang, F.; Stuecker, M.F.; Jin, F.-F.; Timmermann, A. Spurious North Tropical Atlantic precursors to El Niño. *Nat. Commun.* **2021**, *12*. [[CrossRef](#)] [[PubMed](#)]
45. Sample, T.; Xie, S. Large-Scale Dynamics of the Meiyu-Baiu Rainband: Environmental Forcing by the Westerly Jet. *J. Clim.* **2010**, *23*, 113–134. [[CrossRef](#)]

46. Kong, W.; Chiang, J.G.H. Interaction of the Westerlies with the Tibetan Plateau in Determining the Mei-Yu Termination. *J. Clim.* **2020**, *33*, 339–363. [[CrossRef](#)]
47. He, C.; Zhou, T.; Zhang, L.; Chen, X.; Zhang, W. Extremely hot East Asia and flooding western South Asia in the summer of 2022 tied to reversed flow over Tibetan Plateau. *Clim. Dynam.* **2023**. [[CrossRef](#)]
48. Huang, P.; Xie, S. Mechanisms of change in ENSO-induced tropical Pacific rainfall variability in a warming climate. *Nat. Geosci.* **2015**, *8*, 922–926. [[CrossRef](#)]
49. Dai, P.; Nie, J. What Controls the Interannual Variability of Extreme Precipitation? *Geophys. Res. Lett.* **2021**, *48*, e2021GL095503. [[CrossRef](#)]
50. Zhao, P.; Zhang, X.; Zhou, X.; Ikeda, M. The sea ice extent anomaly in the North Pacific and its impact on the East Asian summer monsoon rainfall. *J. Clim.* **2004**, *17*, 3434–3447. [[CrossRef](#)]
51. Alexander, M.A.; Bhatt, U.S.; Walsh, J.E.; Timlin, M. The atmospheric response to realistic Arctic sea ice anomalies in an AGCM during winter. *J. Clim.* **2004**, *17*, 890–905. [[CrossRef](#)]
52. Vihma, T. Effects of Arctic sea ice decline on weather and climate: A review. *Surv. Geophys.* **2014**, *35*, 1175–1214. [[CrossRef](#)]
53. Gong, D.-Y.; Yang, J.; Kim, S.-J.; Gao, Y.; Guo, D.; Zhou, T.; Hu, M. Spring Arctic Oscillation-East Asian summer monsoon connection through circulation changes over the western North Pacific. *Clim. Dyn.* **2011**, *37*, 2199–2216. [[CrossRef](#)]
54. He, S.; Gao, Y.; Li, F.; Wang, H.; He, Y. Impact of Arctic Oscillation on the East Asian climate: A review. *Earth-Sci. Rev.* **2017**, *164*, 48–62. [[CrossRef](#)]
55. Sheng, B.; Wang, H.; Li, H.; Li, Q. Thermodynamic and Dynamic Effects of Anomalous Dragon Boat Water over South China in 2022. 2022. Available online: <https://ssrn.com/abstract=4264758> (accessed on 15 February 2023).
56. Zhu, Y.; Wang, T.; Ma, J. Influence of internal decadal variability on the summer rainfall in eastern China as simulated by CCSM4. *Adv. Atmos. Sci.* **2016**, *33*, 706–714. [[CrossRef](#)]

Disclaimer/Publisher’s Note: The statements, opinions and data contained in all publications are solely those of the individual author(s) and contributor(s) and not of MDPI and/or the editor(s). MDPI and/or the editor(s) disclaim responsibility for any injury to people or property resulting from any ideas, methods, instructions or products referred to in the content.